ORIGINAL ARTICLE

The effect of time-of-flight and point spread function modeling on ^{82}Rb myocardial perfusion imaging of obese patients

Paul K. R. Dasari, PhD,[a] Judson P. Jones, PhD,[b] Michael E. Casey, PhD,[b] Yuanyuan Liang, PhD,[c] Vasken Dilsizian, MD,[a] and Mark F. Smith, PhD[a]

[a] Department of Diagnostic Radiology and Nuclear Medicine, University of Maryland School of Medicine, Baltimore, MD
[b] Siemens Healthineers, Knoxville, TN
[c] Department of Epidemiology and Public Health, University of Maryland School of Medicine, Baltimore, MD

Received May 12, 2017; accepted Apr 13, 2018
doi:10.1007/s12350-018-1311-y

Background. **The effect of time-of-flight (TOF) and point spread function (PSF) modeling in image reconstruction has not been well studied for cardiac PET. This study assesses their separate and combined influence on ^{82}Rb myocardial perfusion imaging in obese patients.**

Methods. **Thirty-six obese patients underwent rest-stress ^{82}Rb cardiac PET. Images were reconstructed with and without TOF and PSF modeling. Perfusion was quantitatively compared using the AHA 17-segment model for patients grouped by BMI, cross-sectional body area in the scanner field of view, gender, and left ventricular myocardial volume. Summed rest scores (SRS), summed stress scores (SSS), and summed difference scores (SDS) were compared.**

Results. **TOF improved polar map visual uniformity and increased septal wall perfusion by up to 10%. This increase was greater for larger patients, more evident for patients grouped by cross-sectional area than by BMI, and more prominent for females. PSF modeling increased perfusion by about 1.5% in all cardiac segments. TOF modeling generally decreased SRS and SSS with significant decreases between 2.4 and 3.0 (P<.05), which could affect risk stratification; SDS remained about the same. With PSF modeling, SRS, SSS, and SDS were largely unchanged.**

Conclusion. **TOF and PSF modeling affect regional and global perfusion, SRS, and SSS. Clinicians should consider these effects and gender-dependent differences when interpreting ^{82}Rb perfusion studies. (J Nucl Cardiol 2018;25:1521–45)**

Spanish Abstract

Antecedentes. **El efecto de los algoritmos de reconstrucción “time of flight” (TOF) y “point spread function” (PSF) en la reconstrucción de imágenes no ha sido bien estudiado para el PET cardiaco. Este estudio evalúa su influencia en por separado y combinado en los estudios de imagen de perfusión miocárdica con ^{82}Rb en pacientes obesos.**

Electronic supplementary material The online version of this article (https://doi.org/10.1007/s12350-018-1311-y) contains supplementary material, which is available to authorized users.

The authors of this article have provided a PowerPoint file, available for download at SpringerLink, which summarises the contents of the paper and is free for re-use at meetings and presentations. Search for the article DOI on SpringerLink.com.

JNC thanks Erick Alexanderson MD, Carlos Guitar MD, and Diego Vences MD, UNAM, Mexico, for providing the Spanish abstract; Haipeng Tang MS, Zhixin Jiang MD, and Weihua Zhou PhD, for providing the Chinese abstract; and Jean-Luc Urbain, MD, PhD, CPE, Past President CANM, Chief Nuclear Medicine, Lebanon VAMC, PA, for providing the French abstract.

Reprint requests: Mark F. Smith, PhD, Department of Diagnostic Radiology and Nuclear Medicine, University of Maryland School of Medicine, 22 South Greene St., Baltimore, MD 21201, *msmith7@umm.edu*

1071-3581/$34.00

Métodos. **Treinta y seis pacientes obesos fueron sometidos a un PET cardiaco ^{82}Rb en estrés y en reposo. Las imágenes fueron reconstruidas con y sin TOF y PSF. La perfusión fue comparada cuantitativamente utilizando el modelo segmentario AHA17 para pacientes agrupados por IMC, área corporal transversal in el campo de vista del escáner, sexo y volumen ventricular izquierdo miocárdico. Los puntajes sumados de reposo (SRS), los puntajes sumados de estrés (SSS) y el puntaje diferencial sumado (SDS) fueron comparados.**

Resultados. **El TOF mejoró la uniformidad visual del mapa polar e incrementó la perfusión de la pared septal hasta un 10%. Este incremento fue mayor para pacientes más grandes, más evidentemente en pacientes agrupados por área transversal que por IMC, y siendo más prominente en mujeres. El PSF aumentó la perfusión por cerca de 1.5% en todos los segmentos cardiacos. El TOF generalmente disminuyó el SRS y el SSS con disminuciones significativas entre 2.4 y 3 (*P*<.05), lo cual podría afectar la estratificación por riesgo; el SDS permanece igual. Con el modelamiento PSF, el SRS, el SSS y el SDS no presentaron cambios.**

Conclusión. **El TOF y el PSF afecta a la perfusión regional y global, el SRS y el SSS. Los clínicos deberían considerar estos efectos y las diferencias dependientes de sexo cuando se interpretan los estudios de perfusión con ^{82}Rb. (J Nucl Cardiol 2018;25:1521–45)**

Chinese Abstract

背景. 飞行时间**(TOF)**和点扩散函数**(PSF)**建模对于心脏 PET 成像重建的影响尚未完善建立。本研究评估其单独以及联合使用对肥胖病人行铷 **82** 心肌灌注成像的影响。

方法. **36** 个肥胖病人接受静息-负荷的铷 **82** 心脏 **PET** 成像扫描。图像分别在有无 **TOF** 和 **PSF** 建模的情况下被重建。病人按照 **BMI**、扫描仪视野下横断面的体表面积、性别和左室容积进行分组,采用 **AHA 17**节段模型量化对比灌注情况,比较静息灌注总积分**(SRS)**,负荷灌注总积分**(SSS)**和灌注总积分差值**(SDS)**。

结果. **TOF** 改进了靶心图的视觉一致性, 间隔壁的灌注增加了**10%**。这种增加表现为**:** 体型越大的病人增加越大, 以横断面体表面积分组的病人比用 **BMI** 分组的病人增加更明显,女性比男性增加更突出。在所有的心脏节段中, **PSF** 建模增加了约 1.5% 的灌注。**TOF** 建模总体上显著降低了**SRS**和 **SSS**(在 **2.4** 和 **3.0** 之间, ***P*<.05**), 这会影响风险分层**; SDS** 保持不变。利用 **PSF** 建模**, SRS, SSS** 和 **SDS** 在很大程度上保持不变。

结论. **TOF** 和 **PSF** 建模影响局部和整体灌注、**SRS** 以及 **SSS**。当阅读铷 **82** 灌注图像时,临床医生应该考虑这些因素的影响以及性别导致的不同。 **(J Nucl Cardiol 2018;25:1521–45)**

French Abstract

Contexte. **L'effet de la modélisation du temps de vol (TOF) et de la fonction d'étalement ponctuel (PSF) pour la reconstruction d'images n'a pas été bien étudiée pour la TEP en cardiologie. Cette étude évalue l'influence séparée et combinée des ces deux facteurs sur la perfusion myocardique par imagerie au ^{82}Rb chez les patients obèses.**

Méthodes. **Trente-six patients obèses ont été soumis à une étude TEP repos-effort au ^{82}Rb au repos. Les images ont été reconstruites avec et sans modélisation TOF et PSF. Les résultats de la perfusion myocardique a été comparée quantitativement en utilisant le modèle de 17 segments de l'American Heart Association (AHA). Les patients ont été groupés selon l'index de leur masse corporelle (IMC), et selon leur dimension corporelle transversale dans le champ de vision du scanner, sexe et volume myocardique ventriculaire gauche. Les score de perfusion myocardique au repos (SRS), après effort (SSS) et les scores différentiels (SDS) ont été comparés.**

Résultats. **TOF améliore l'uniformité visuelle de la carte polaire et augmente la perfusion de la paroi septale de 10%. Cette augmentation est plus importante chez les patients de grande taille et plus apparente chez les patients groupés selon leur dimension corporelle transversale zone plutôt que par l'IMC, et plus élevée chez les femmes. La modélisation PSF augmente la perfusion d'environ 1,5% dans tous les segments cardiaques. La modélisation TOF diminue**

significativement les scores SRS et le SSS de 2,4 et 3,0 points (*P*<0,05), ce qui peut changer la stratification; le score SDS est dans l'ensemble inchangé. Avec la modélisation PSF, SRS, SSS et SDS sont largement inchangés.

Conclusion. **La modélisation TOF et PSF affectent la perfusion régionale et globale, SRS et SSS. Les cliniciens devraient tenir compte de ces effets et des différences entre les sexes lors de l'interprétation ^{82}Rb études de perfusion. (J Nucl Cardiol 2018;25:1521–45)**

Key Words: Coronary artery disease · image reconstruction · myocardial perfusion imaging · obese · PET · time-of-flight · point spread function · ^{82}Rb

Abbreviations

BMI	Body mass index
CAD	Coronary artery disease
FWHM	Full-width at half-maximum
FOV	Field of view
LMM	Linear mixed effects model
LV	Left ventricular/left ventricle
MPI	Myocardial perfusion imaging
OSEM	Ordered subsets expectation maximization
OSEMTOF	OSEM reconstruction with TOF modeling
PET	Positron emission tomography
PSF	Point spread function/OSEM reconstruction with PSF modeling
PSFTOF	OSEM reconstruction with TOF and PSF modeling
SDS	Summed difference score
SNR	Signal-to-noise ratio
SPECT	Single-photon emission computed tomography
SRS	Summed rest score
SSS	Summed stress score
TOF	Time-of-flight

See related editorials, pp. 1546–1549 and pp. 1550–1553

INTRODUCTION

Myocardial perfusion imaging (MPI) with positron emission tomography (PET) has gained increasing interest due to superior image quality over single-photon emission computed tomography (SPECT) and improved diagnostic accuracy owing to higher spatial resolution and correction for attenuation and scatter.[1,2] Obese patients represent a growing amount of patients undergoing evaluation for coronary artery disease (CAD) and the most common myocardial perfusion PET tracer, rubidium-82 (^{82}Rb), has demonstrated high sensitivity,[3] specificity, [4] and improved diagnostic accuracy[1,5] for the detection of CAD among these patients. A recent study of ^{82}Rb PET comparing obese (body mass index (BMI)≥ 30 kg/m^2) with overweight (BMI 25-30 kg/m^2) and normal (BMI<25 kg/m^2) patients showed that the prognostic value remained the same irrespective of BMI.[6]

Advanced PET image reconstruction methods include time-of-flight (TOF) and point spread function (PSF) modeling. The influence of TOF has been studied mainly for oncology, where phantom and patient data have demonstrated better image quality, improved accuracy and precision of regional quantification, and increased contrast and signal-to-noise ratio (SNR), particularly for obese patients.[7–12] TOF images are less susceptible to artifacts due to inconsistent data used for detector normalization, scatter, and attenuation correction.[13–15] PSF modeling in iterative reconstruction provides more accurate activity estimates,[16–18] decreases image noise and reduces partial-volume effects, though it may cause edge artifacts and alter image noise.[18–20] PSF modeling improves image quality of cardiac ^{18}F fluorodeoxyglucose viability (average BMI 28.3±5.9) and ^{82}Rb perfusion studies (average BMI 25.3±6.5).[21]

Phantom and patient studies with TOF and PSF modeling have demonstrated promising results for ^{82}Rb cardiac PET,[21–24] including obese patients;[23] however, the magnitude of these effects for both normal and obese patients has not been well studied. Armstrong et al[22] showed that TOF+PSF reconstruction resulted in greater flow values compared with OSEM, though myocardial flow reserve (MFR) was not affected. The separate influences of TOF and PSF were not studied, but these authors did show an example (their Figure 6) of increased flow in the septal wall of PSF+TOF compared with OSEM. In a study of 27 subjects, Oldan et al [25] found no significant overall or segmental differences between FDG cardiac images reconstructed with and without TOF. Examples of the differences between TOF and non-TOF ^{82}Rb cardiac reconstructions (both with PSF) for two obese patients are shown by DiFilippo et al[23] (their Figures 2, 3). In a study of SNR for small tumors, the SNR improvement with TOF observed in abdominal and head and neck regions as BMI increases does not hold true in the lungs.[9] Cardiac SNR results reported recently by Armstrong et al[26] are consistent with this observation and show that improvement in SNR in the myocardium is independent of BMI. As Wells and de Kemp note in an accompanying editorial,[27] cardiac imaging with relatively intense uptake compared to low lung background is different in nature from a homogenous activity region from which early theoretical predictions of the effect of SNR improvement with TOF were derived,[28] and further study is needed to address the potential benefit of TOF in cardiac imaging. Theoretical analyses of the potential SNR improvements with TOF are further complicated by the routine clinical use of iterative reconstruction algorithms with improved SNR characteristics vs. analytic filtered backprojection algorithms.

In a previous investigation using average and large anthropomorphic cardiac-torso phantoms, we found that TOF and PSF modeling improved tracer quantitation accuracy and uniformity in the myocardial wall, especially for the phantom representing an obese patient.[29]

This article presents results on the individual and combined effects of TOF and PSF modeling on myocardial perfusion as a function of patient BMI and cross-sectional area of transaxial slices containing the heart. Breast tissue in the field of view and the size of the heart may influence the effects of TOF and PSF modeling, motivating analysis by gender and left ventricular (LV) myocardial volume.

Table 1. Patient demographics

Variable	Male (*N*=9)	Female (*N*=27)	Total (*N*=36)	*P* value
Weight (kg)				0.03[1]*
Mean± SD	164.02±41.88	127.06±22.07	136.3±32.03	
Median [Q1, Q3]	171.82 [136.36, 186.82]	128.23 [107.27, 142.3]	136.82 [113.5, 149.76]	
Min, max	105, 225.45	85.6, 174.09	85.6, 225.45	
BMI (kg/m^2)				0.67[1]
Mean± SD	50.06±13.31	46.57±8.06	47.44±9.54	
Median [Q1, Q3]	51.47 [38.6, 55.6]	46.4 [40.51, 52.79]	46.48 [39.82, 53.87]	
Min, max	36.01, 75.57	32.46, 63.87	32.46, 75.57	
LV myocardial volume (mL)				< 0.001[1]*
Mean± SD	148.78±55.53	65.44±31.34	86.28±52.66	
Median [Q1, Q3]	146.5 [112, 190]	56.5 [44.25, 82]	74.25 [48.12, 100.75]	
Min, max	79, 237.5	18.5, 171.5	18.5, 237.5	
Area, transaxial slice containing the heart (cm^2)				0.67[1]
Mean± SD	1141.74±325.62	1139.89±182.41	1140.35±221.25	
Median [Q1, Q3]	1086.14 [905.49, 1288.29]	1140.97 [1063.53, 1188.57]	1134.38 [1046.97, 1263.06]	
Min, max	732.99, 1662.26	531.86, 1548.27	531.86, 1662.26	
Age (year)				0.56[1]
Mean± SD	54.33±7.21	56.44±9.78	55.92±9.15	
Median [Q1, Q3]	56 [48, 58]	57 [50.5, 63]	56.5 [49.75, 62.25]	
Min, max	44, 65	37, 82	37, 82	

**P* value<.05
[1]Mann-Whitney *U* test
[2]Fisher's exact test

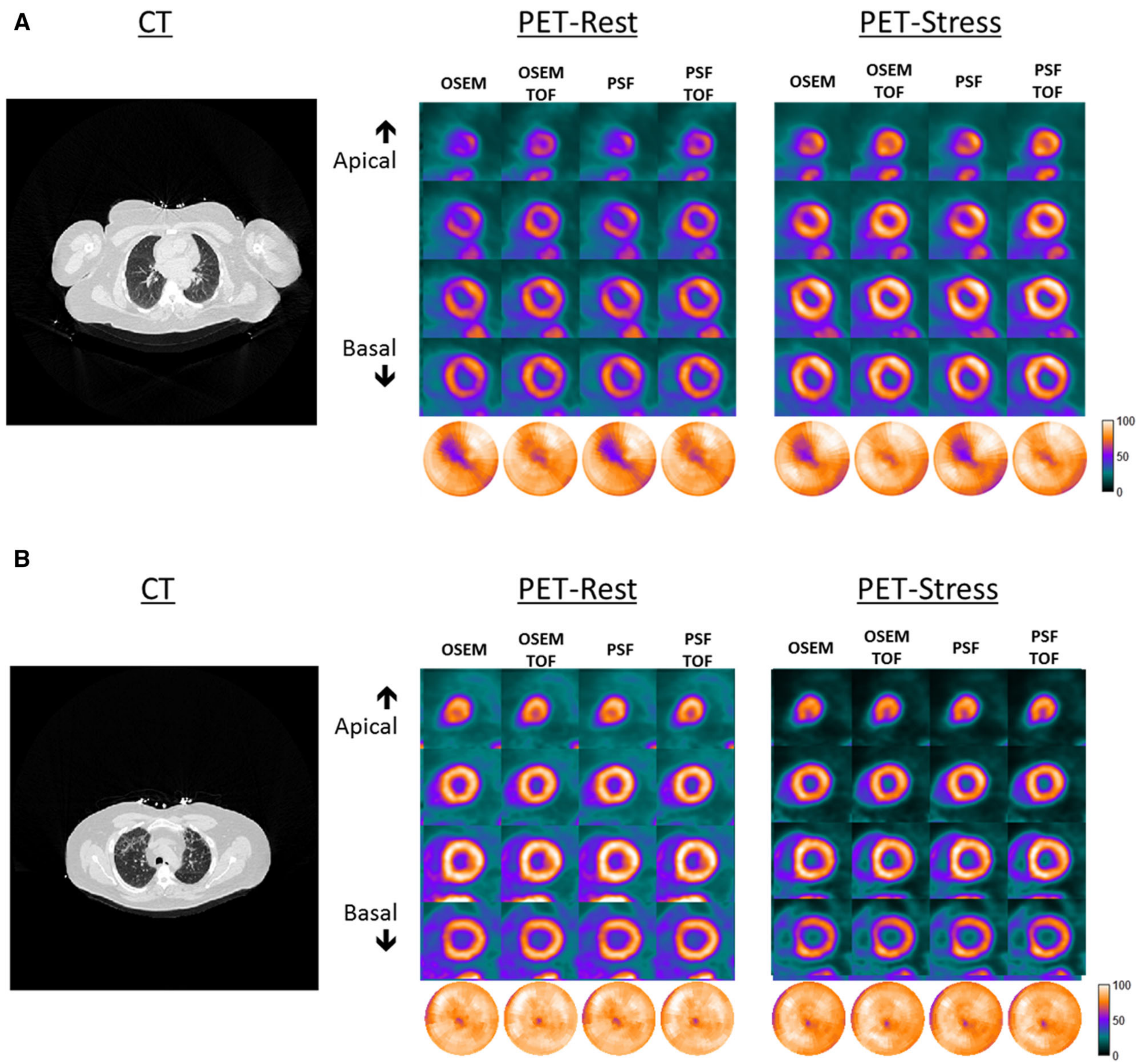

Figure 1. Transaxial CT slice, short-axis slices, and polar maps of rest-stress ^{82}Rb PET MPI for two patients and the four reconstruction algorithms. (**A**) Subject 5, female, with BMI 38.5 kg/m^2 and cross-sectional area 1342 cm^2, and (**B**) subject 4, male, with BMI 36.0 kg/m^2 and cross-sectional area 905 cm^2.

MATERIALS AND METHODS

Study Population

Thirty-six patients referred for assessment of CAD with ^{82}Rb PET MPI at the University of Maryland Medical Center were included in the study on a rolling basis as they met enrollment criteria of weight>113.6 kg (250 lb) or BMI>30 and provided informed consent under a protocol approved by the University of Maryland, Baltimore Institutional Review Board. Patient demographics are given in Table 1.

^{82}Rb PET/CT Acquisition

Rest and pharmacological stress ^{82}Rb PET MPI was performed on a Siemens Biograph mCT PET/CT scanner with four rings of block detectors and a 21.6 cm axial PET field of view.[30] Patients were instructed to abstain from caffeine products for 12 h prior to the study. Imaging was performed with arms above the head unless this could not be tolerated. First, a CT scan for attenuation correction was performed under free breathing over a 22.4 cm axial field of view. Scan parameters were x-ray tube voltage 120 kVp, tube current

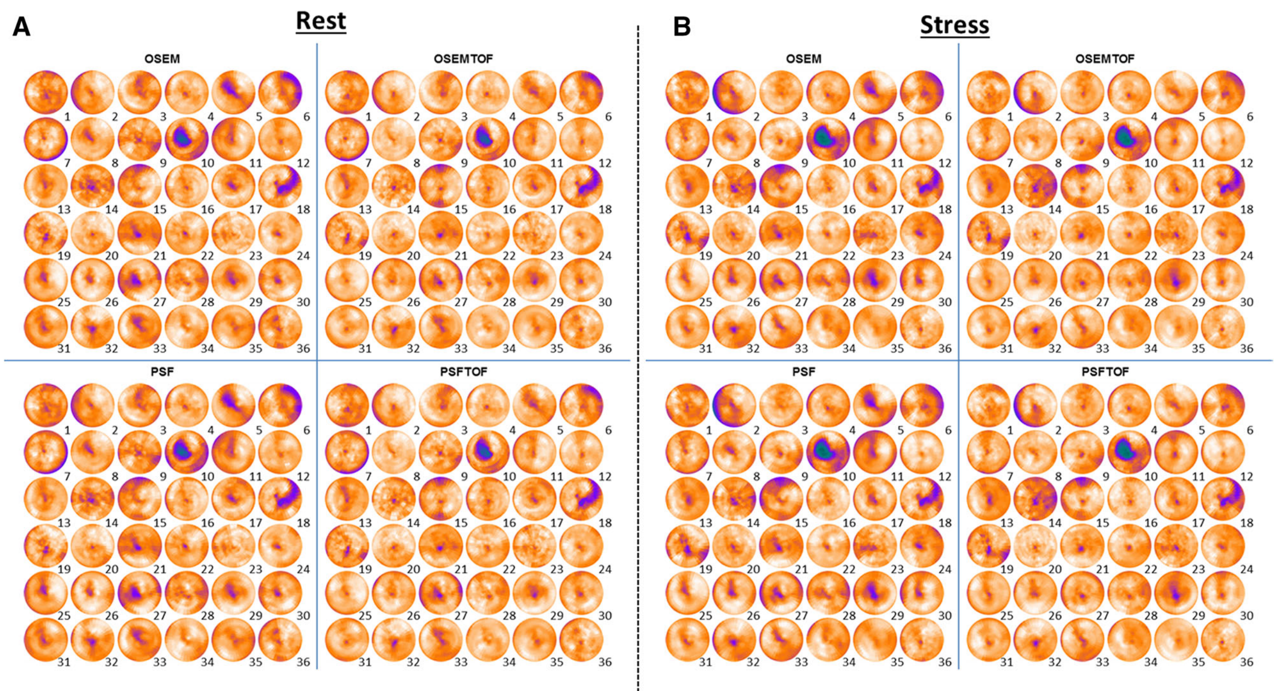

Figure 2. (**A**) Rest and (**B**) stress polar maps for OSEM, OSEMTOF, PSF, and PSFTOF reconstructions for the 36 study subjects.

300 mA, exposure time 500 ms, total collimation width 19.2 mm, table speed 57.6 mm/seconds, table feed per rotation 28.8 mm, and pitch factor 1.5. The $CTDI_{vol}$ was 7.28 mGy and the dose-length product was 174 mGy·cm.

Next, two 8-minute 3D listmode PET studies were performed at rest and under pharmacological stress with adenosine or regadenoson. Activity was administered from a Cardiogen ^{82}Sr-^{82}Rb generator (Bracco Diagnostics). The activity administration parameters were a maximum administered activity of 2220 MBq (60 mCi), maximum flow rate of 50 mL/minute, and a maximum injected volume of 50 mL. Weight-dependent dosing was not performed. The actual injected activity (mean ± SD) for each scan was 1974 ± 312 MBq (53.3 ± 8.4 mCi) with a range of 1095-2231 MBq (29.5-60.3 mCi) and a median of 2203 MBq (59.6 mCi). The smallest amounts of activity (~1110-1480 MBq; ~30-40 mCi) were administered when the generator was the oldest (~40 days old; the half-life of ^{82}Sr is 25.3 days) and the dose volume reached the 50 mL limit.

Detector saturation is a concern for large administered doses and fan sum plots showing the coincidence events for each detector block can show saturation and stunning effects.[31] The fan sum plots were examined in different time frames for each study. Although there is evidence of dose saturation in some detector blocks for a few patients at early times, no saturation effects were observed during the 1.5-8.0 minute period that was used for generation of the perfusion images.

Registration of PET and CT images was checked by the technologist and adjusted via manual rigid-body registration if necessary. PET and CT data were anonymized and transferred to a workstation equipped with Siemens e7 software tools, enabling offline image reconstruction with clinical algorithms.

Image Reconstruction

Static perfusion images were reconstructed using data from 1.5-8 minute post-injection using four different algorithms. These were (1) Ordered Subsets Expectation Maximization (OSEM), (2) OSEM with TOF (OSEMTOF), (3) OSEM with PSF modeling (PSF), and (4) OSEM with PSF modeling and TOF (PSFTOF). The data were corrected for normalization, randoms, scatter, prompt gamma rays, dead time losses, and attenuation. The manner of implementation of corrections for scatter and prompt gamma rays may be found in Refs.[32,33]. PSF modeling used the HD-PET option (Siemens Medical Solutions).[16] All iterative reconstructions were performed with 4 iterations, 21 subsets, and an 8-mm full width at half maximum (FWHM) 3D Gaussian post-reconstruction filter, which matches clinical practice for ^{82}Rb TOF image reconstructions.

Image Processing and Analysis

Polar maps of perfusion were generated using PMOD (PMOD Technologies), which extracted peak values (Bq/mL) in the LV myocardium along rays perpendicular to the long axis of the LV. There were 36 samples at 10-degree angular increments in each of 21 equally spaced slices from apex to base plus a single sample at the apex.

Qualitative and quantitative analyses were performed to assess the effects of TOF and PSF modeling. The short-axis images and polar maps were scaled to their own maximum value only for qualitative display.

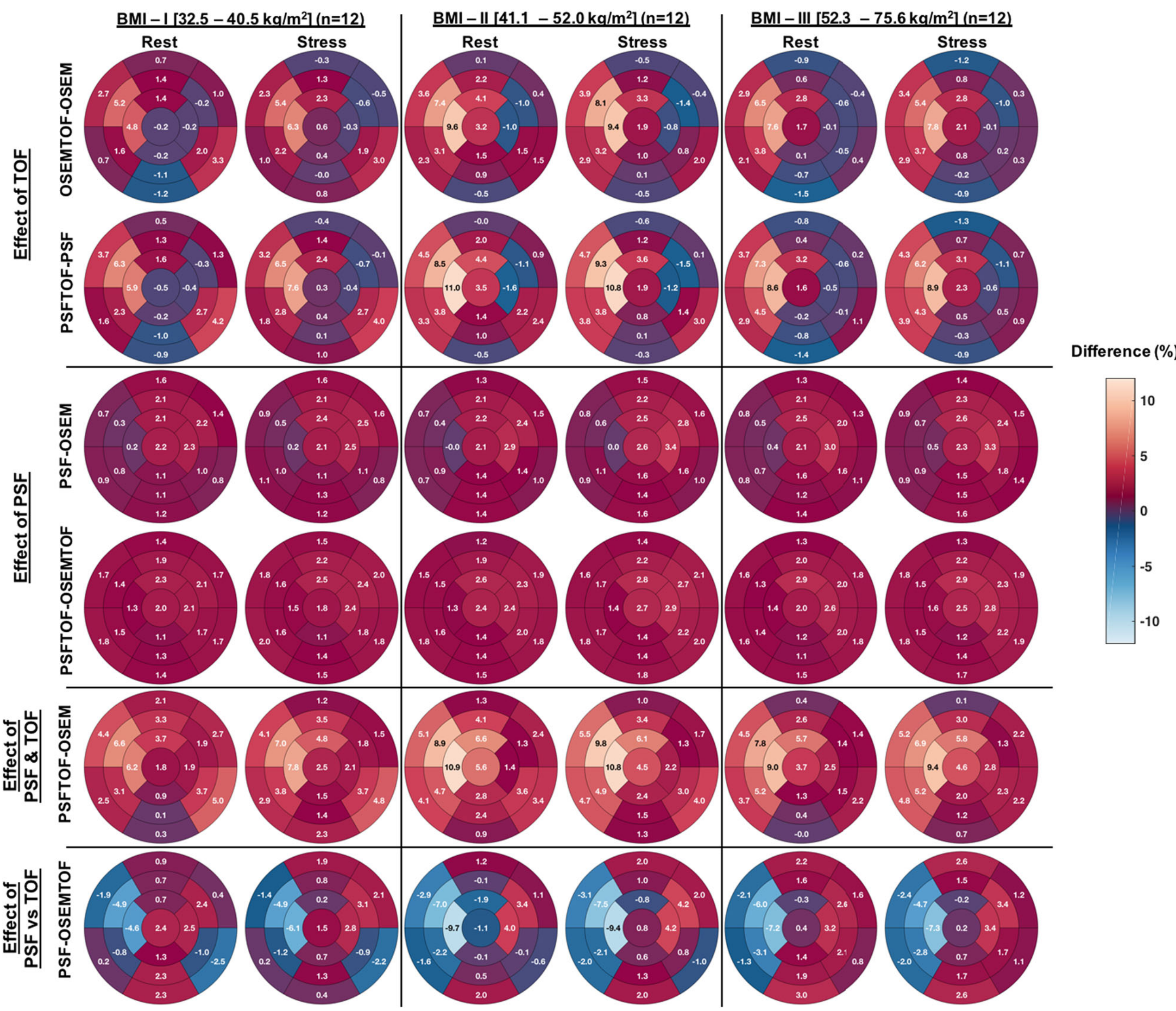

Figure 3. 17-segment polar maps of segmental differences in cardiac perfusion between the different reconstructions for patients grouped by BMI. The values for non-significant changes are given in white font while significant changes are given in black font.

Quantitative analysis was performed using the polar map values of absolute activity concentrations (Bq/mL). These were first averaged in the 17 segments of the American Heart Association (AHA) heart model.[34] The effect of applying TOF, PSF or both was computed using segmental data normalized to the maximum (peak perfusion) segmental value from OSEM (algorithm (1)). The mean percent change in segmental perfusion relative to OSEM is given by

$$(\%\,\mathrm{Change})_i = \frac{1}{N}\sum_{n=1}^{N}\left(\frac{\mathrm{Segment}_{M,n}(i) - \mathrm{Segment}_{\mathrm{OSEM},n}(i)}{\mathrm{Max}\{\mathrm{Segment}_{\mathrm{OSEM},n}(j) := 1,\ldots,17\}}\right) \times 100, \qquad (1)$$

where n=patient number, N =number of patients, i = AHA segment number, M =reconstruction algorithm with TOF and/or PSF.

Differences in segmental perfusion were analyzed according to patient BMI and body cross-sectional area in the field of view (FOV) of the scanner. The latter was motivated by the fact that a small, obese patient could have a high BMI yet not have a large body area in the PET FOV. Errors in scatter and attenuation correction, and the influence of TOF, will likely be greater when there is more body mass in the FOV. The patient cross-sectional area in a transaxial slice through the heart was determined by segmenting a reconstructed x-ray CT slice into air and non-air components using MATLAB (Mathworks). The

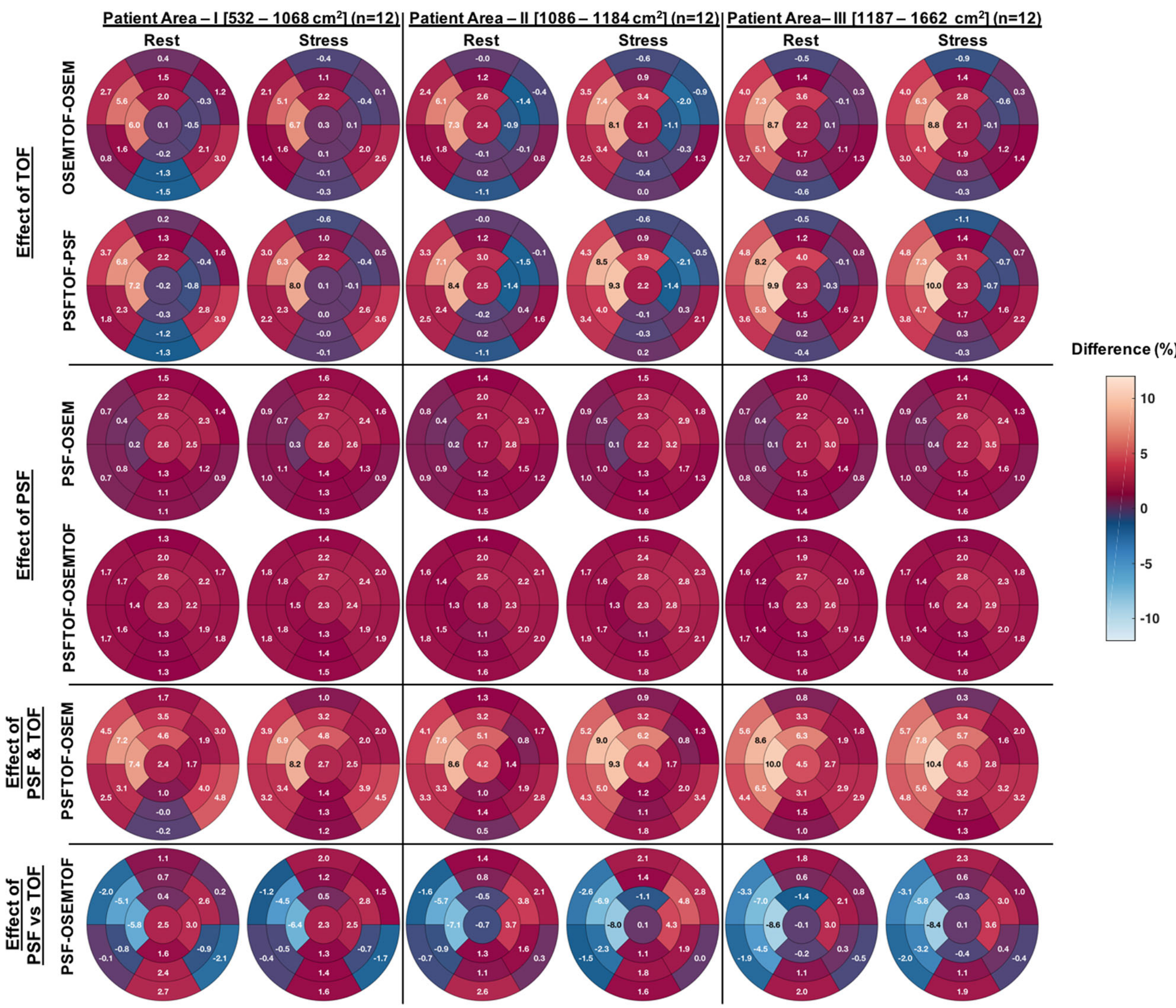

Figure 4. 17-segment polar maps of segmental differences in cardiac perfusion between the different reconstructions for patients grouped by cross-sectional area in the PET FOV. The values for non-significant changes are given in white font while significant changes are given in black font.

voxels inside the outer body contour and inside the arm(s) (if in the field of view) were counted and used to compute the cross-sectional area. The perfusion data also were analyzed with respect to gender and LV myocardium size. The LV myocardial volume was determined by Corridor 4DM (INVIA) from automatically determined epicardial and endocardial contours.[35] Due to the non-linear associations between continuous predictors (such as BMI) and the outcomes, patients were grouped based on tertiles, each with 12 patients, to evaluate whether perfusion changes were associated with the magnitude of BMI groups (<41, 41-52.1,>52.1 kg/m^2), cross-sectional area groups (<1070, 1070-1186,>1186 cm^2), and LV myocardial volume groups (<54, 54-87, >87 mL), respectively.

Summed stress score (SSS), summed rest score (SRS), and summed difference score (SDS)[36] were automatically computed as in Ref. [37,38] for each patient and each reconstruction method. Using the 17-segment model, uptake in each segment was normalized to the maximum segment value for that study and multiplied by 100. Each segment was scored as 0=normal uptake (85-100%), 1=mild decrease (70-85%), 2=moderate decrease (50-70%), 3=severe decrease (15-50%), and 4=no uptake (0-15%). SSS, SRS, and SDS were computed and analyzed according to patient BMI, cross-sectional area, gender, and LV size.

Statistical Analysis

Summary statistics for demographic data were reported and compared by gender, BMI groups, cross-sectional area groups, and LV size groups, respectively, using Mann-Whitney U test or Kruskal-Wallis H test for continuous variables and Fisher's exact test for categorical variables as appropriate. For each summed score (SSS, SRS, and SDS), linear mixed effects models (LMMs) were used to compare the four reconstruction algorithms (OSEM, OSEMTOF, PSF, PSFTOF) with and without adjusting for gender, BMI groups, cross-sectional area groups, and LV size groups, respectively, while taking into account the correlation among the measures from the same patient. The model-based pairwise comparisons among the four reconstruction algorithms were examined using Scheffé's method.

Similarly, for the segmental data from rest and stress studies, LMMs were used to compare the four reconstruction algorithms while adjusting for segments and each demographic data of interest (i.e., gender, BMI groups, cross-sectional area groups, and LV size groups). The model-based pairwise comparisons among the four reconstruction algorithms within each segment were examined using Scheffé's method. All statistical tests were performed with a two-sided significance level of 0.05. All analyses were performed using Stata/SE (version 15, Stata Corporation).

The percent change for each segment was displayed in an AHA 17-segment polar map. The values for non-significant

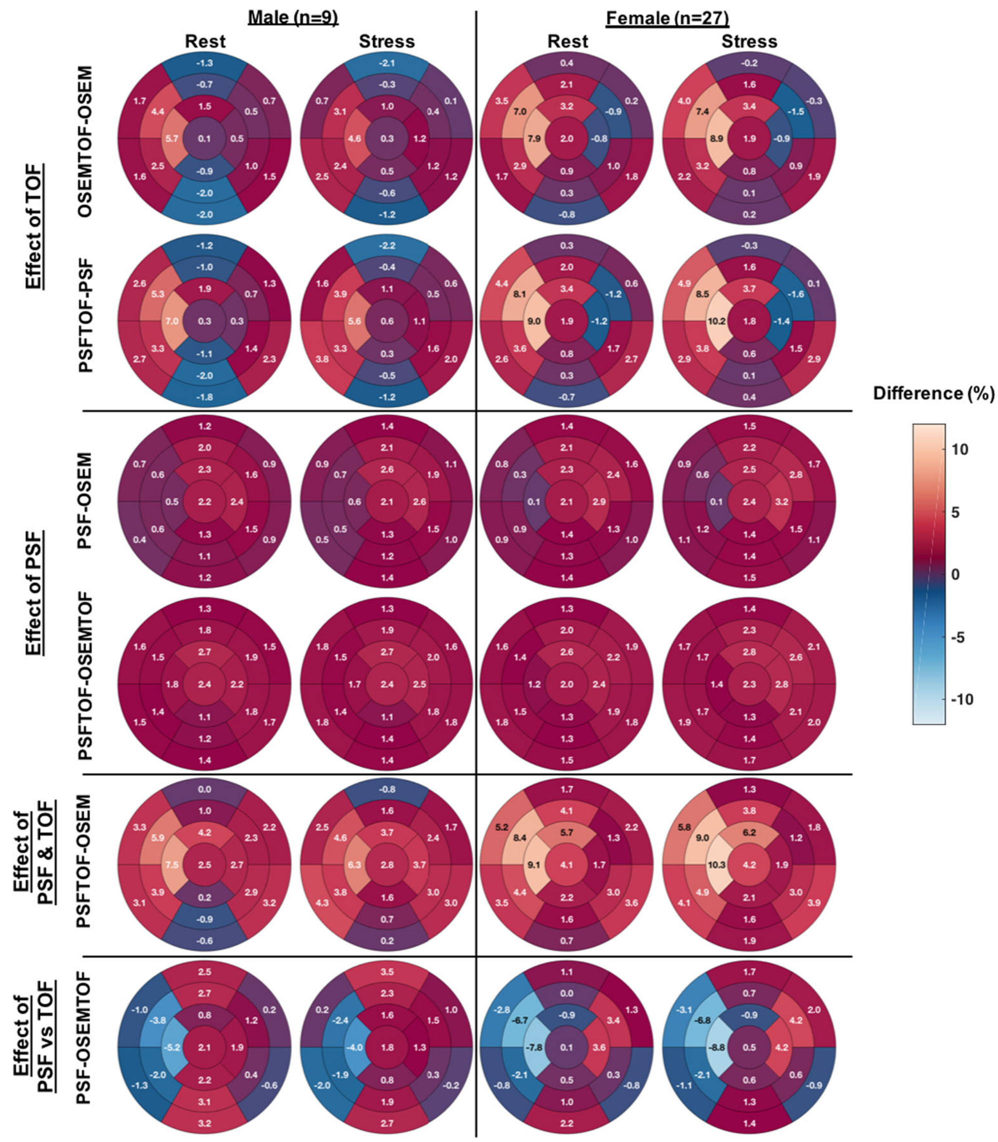

Figure 5. 17-segment polar maps of segmental differences in cardiac perfusion between the different reconstructions for males and females. The values for non-significant changes are given in white font while significant changes are given in black font.

changes are given in a white font while significant changes are given in a black font.

RESULTS

Qualitative Analysis

Short-axis cardiac images and polar maps for two representative subjects are shown in Figure 1 and polar maps for the four iterative reconstruction methods for all subjects are shown in Figure 2. Low perfusion regions are less prominent and polar maps are more uniform with TOF (Figure 1). The latter observation applies to polar maps from all patients (Figure 2). In this study, 11 out of 36 patients had one (patients 15, 22) or both (patients 5, 11, 25, 26, 27, 29, 33, 34, 35) arms in the FOV. With TOF reconstruction, the size and intensity of apparent perfusion defects are often reduced and in general perfusion appears higher in the septal wall.

Quantitative Analysis, Segmental Uptake

The percentage differences in myocardial uptake between (a) TOF and non-TOF (OSEMTOF-OSEM, and OSEMTOF-PSF), (b) PSF and non-PSF (PSF-OSEM and PSFTOF-OSEMTOF), (c) PSFTOF and OSEM (PSFTOF-OSEM), and (d) PSF only and TOF only (PSF-OSEMTOF) algorithms categorized by BMI, patient cross-sectional area, gender, and LV size are

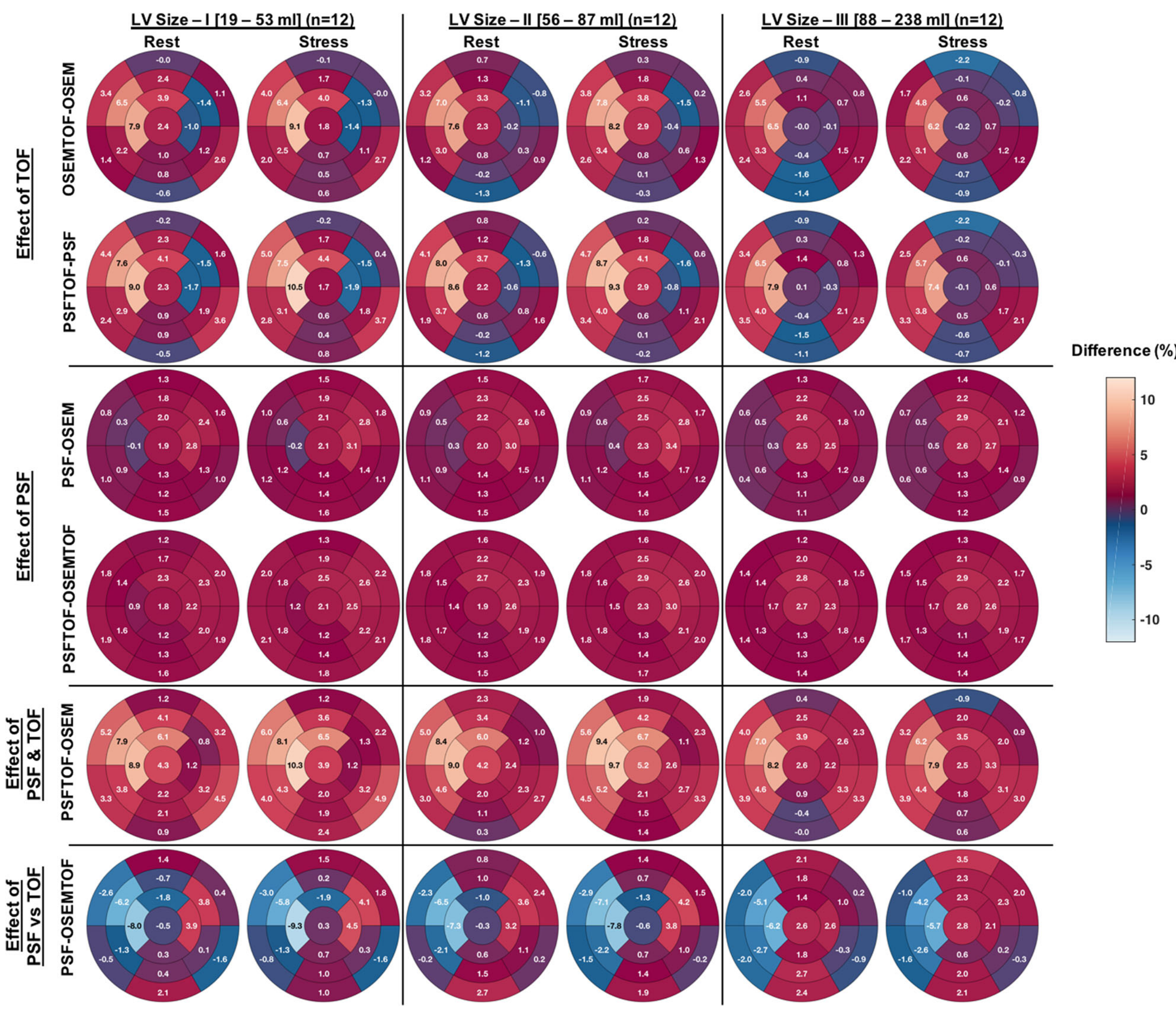

Figure 6. 17-segment polar maps of segmental differences in cardiac perfusion between the different reconstructions for patients grouped by LV volume. The values for non-significant changes are given in white font while significant changes are given in black font.

Table 2. Patient groups by BMI

Variable	BMI-I (*N*=12)	BMI-II (*N*=12)	BMI-III (*N*=12)	*P* value
Gender				0.32[2]
Male	4	1	4	
Female	8	11	8	
Weight (kg)				< 0.001[1]*
Mean±SD	113.7±18.21	129.86±20.98	165.35±31.15	
Median [Q1, Q3]	106.18 [102.77, 130.77]	125.48 [115.76, 143.42]	153.72 [141.69, 177.27]	
Min, max	85.6, 139.55	98.64, 172.14	128.18, 225.45	
BMI (kg/m^2)				< 0.001[1]*
Mean±SD	37.51±2.83	46.89±3.54	57.92±6.45	
Median [Q1, Q3]	38.55 [35.5, 39.53]	46.48 [44.59, 50.14]	55.46 [54.71, 58.2]	
Min, max	32.46, 40.54	41.1, 52.03	52.27, 75.57	
LV myocardial volume (mL)				0.44[1]
Mean±SD	96.67±71.51	74.58±48.63	87.58±32.82	
Median [Q1, Q3]	67.75 [44.62, 152.75]	69.75 [41.5, 86.62]	82.25 [66.38, 112.38]	
Min, max	18.5, 237.5	30.5, 210.5	48.5, 160.5	
Area, transaxial slice containing the heart (cm^2)				0.001[1]*
Mean±SD	973.09±214.31	1128.98±85.66	1318.99±192.41	
Median [Q1, Q3]	971.65 [889.6, 1113.56]	1124.82 [1065.91, 1163.45]	1310.31 [1152.01, 1440.56]	
Min, max	531.86, 1341.56	995.13, 1288.29	1086.14, 1662.26	
Age (year)				0.84[1]
Mean±SD	56.17±8.5	55.33±8.48	56.25±11.03	
Median [Q1, Q3]	57.5 [54, 63]	54 [49.75, 62.25]	55 [48.75, 60.25]	
Min, max	37, 66	41, 69	43, 82	

**P* value<.05
[1]Kruskal-Wallis *H* test
[2]Fisher's exact test

summarized in 17-segment polar maps (Figures 3, 4, 5, and 6).

General trends are summarized before a detailed analysis by classification scheme. Whole heart perfusion values averaged over the 17 segments were compared with OSEM values. For the rest case, perfusion was 1.9% greater for OSEMTOF, 1.6% greater for PSF, and 3.9% greater for PSFTOF. The differences between each method were significant ($P<.05$) except for PSF vs. OSEMTOF. For the stress case , perfusion was 2.0% greater for OSEMTOF, 1.8% greater for PSF, and 4.2% greater for PSFTOF. The differences between each method were significant ($P<.05$) except for PSF vs. OSEMTOF. The magnitude of the differences for stress was not significantly different than the magnitude of the differences for rest.

Iterative reconstructions with TOF showed marked increased uptake in the septal wall and a slight decrease in the inferior and anterolateral walls. PSF modeling resulted in a small uptake increase in almost all 17 segments. This is consistent with higher values expected with resolution recovery. The change in uptake with PSF was comparable for rest and stress studies. The combined effect of TOF and PSF modeling was approximately additive. Due to the greater magnitude of the increase with TOF compared to that with PSF in some septal segments, the difference polar maps of PSF-OSEMTOF showed negative values in some of these

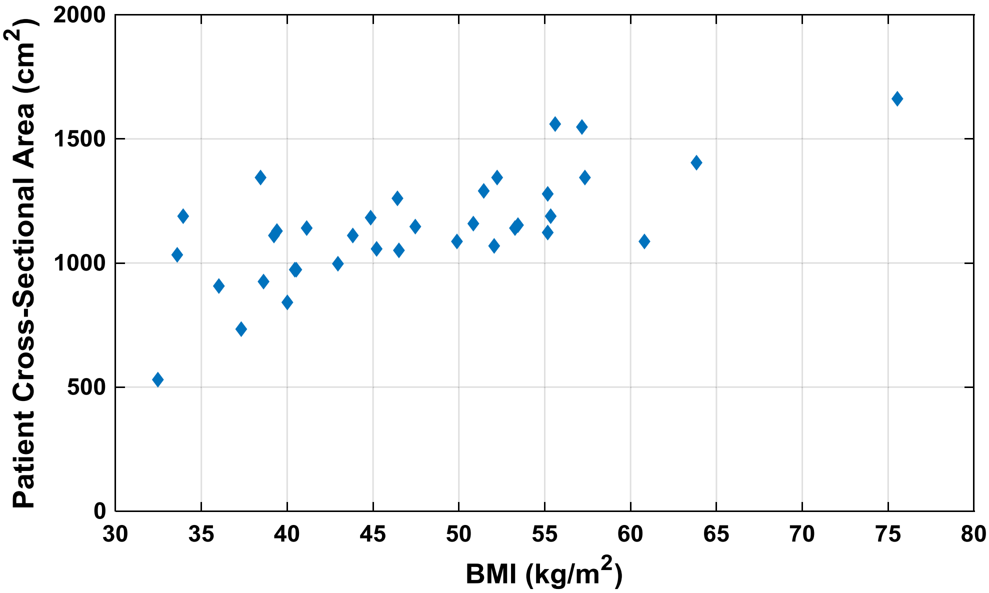

Figure 7. Patient cross-sectional area in the PET scanner field of view vs. BMI.

segments that reached statistical significance. These general trends for TOF and PSF modeling were the same across BMI, cross-sectional area, gender, and LV size groups.

Results by patient BMI. For TOF iterative reconstructions, the change in uptake was greater for the two tertiles with greater BMI, with peak values slightly larger for the BMI-II group (Figure 3). The trend was for increased perfusion throughout the septal wall, though increases reached statistical significance ($P<.05$) only for AHA segments 8 (mid anteroseptal) and 14 (apical septal) walls. When only PSF was modeled in image reconstruction, the change in uptake was comparable among the groups and did not reach statistical significance in any segment. For PSFTOF, the magnitude of the changes was greater than for TOF or PSF alone, reflecting their combined influence, and only reached statistical significance in segments 8 and 14 in BMI-II and BMI-III groups.

Patient characteristics for the BMI tertiles are summarized in Table 2. Not unexpectedly the weight ($P<.001$) and area of the transaxial slice containing the heart ($P<.001$) were significantly different among the BMI tertiles. The distribution of male and female patients was not associated with the BMI group ($P=.32$).

Results by patient cross-sectional area. The observation that the magnitude of uptake changes with TOF was not greater for BMI tertile III than BMI tertile II was initially puzzling. This led us to consider the physical factors leading to changes with TOF. Corrections for attenuation and scatter and the effect of misregistration between emission and transmission scans due to respiration, for example, will be greater when more of the body is in the FOV of the PET scanner. Although body cross-sectional area is related to BMI (Figure 7), short patients could have a high BMI yet have less body area in the scanner than a tall patient with a small BMI. This provided the rationale for evaluating changes due to TOF and PSF as a function of body cross-sectional area in a transaxial slice through the heart.

Patients were grouped into cross-sectional area tertiles and results are shown in Figure 4. For TOF iterative reconstructions, the change in uptake generally increased in patient groups with greater cross-sectional area (Patient Area-III>Patient Area-II>Patient Area-I). As for BMI, the trend was for increased perfusion in the septal wall with statistically significant differences ($P<.05$) only for segments 8 and 14. For reconstructions with PSF modeling, the change in uptake was comparable among patient groups. For PSFTOF, a similar trend as with TOF was observed.

Patient characteristics for the cross-sectional area tertiles are summarized in Table 3. As expected, there were statistically significant differences in weight and BMI among the groups. The differences in LV myocardial volume were not statistically significant. The distribution of male and female patients was not associated with the LV size group ($P=.32$).

Results by gender. For TOF iterative reconstructions, the change in uptake in the septal wall was generally greater for females than males and reached statistical significance for AHA segments 8 (mid anteroseptal) and 14 (apical septal) walls for females,

Table 3. Patient groups by cross-sectional area

Variable	Patient Area-I (*N*=12)	Patient Area-II (*N*=12)	Patient Area-III (*N*=12)	*P* value
Gender				0.32[2]
Male	4	1	4	
Female	8	11	8	
Weight (kg)				0.004[1]*
Mean±SD	116.74±18.73	133.29±23.4	158.87±37.19	
Median [Q1, Q3]	115.66 [103.45, 136.59]	134.06 [114.86, 143.42]	153.72 [137.81, 172.63]	
Min, max	85.6, 141.82	104.09, 186.82	95.45, 225.45	
BMI (kg/m^2)				0.003[1]*
Mean±SD	40.49±5.59	48.28±6.82	53.55±10.86	
Median [Q1, Q3]	40.22 [37.02, 43.54]	48.67 [43.16, 53.34]	55.23 [50.2, 57.22]	
Min, max	32.46, 52.03	39.22, 60.82	33.97, 75.57	
LV myocardial volume (mL)				0.36[1]
Mean±SD	98.46±70.3	66.58±22.38	93.79±52.31	
Median [Q1, Q3]	76.75 [43.38, 152.75]	67.75 [49, 76.62]	85.75 [55.62, 114.25]	
Min, max	30.5, 237.5	38, 112	18.5, 210.5	
Area, transaxial slice containing the heart (cm^2)				< 0.001[1]*
Mean±SD	923.61±157.77	1130.53±29.3	1366.91±150.54	
Median [Q1, Q3]	971.65 [889.6, 1036.25]	1134.38 [1108.67, 1149.46]	1341.96 [1273.2, 1440.56]	
Min, max	531.86, 1068.29	1086.14, 1184.07	1187.09, 1662.26	
Age (year)				0.85[1]
Mean±SD	56.25±9.75	56.17±11.66	55.33±5.9	
Median [Q1, Q3]	57.5 [49.75, 63.5]	52 [49, 63]	56 [52.75, 58.5]	
Min, max	37, 69	41, 82	43, 65	

**P* value<.05
[1]Kruskal-Wallis *H* test
[2]Fisher's exact test

but not for males (see top two rows of polar maps in Figure 5). The effect of PSF modeling was a slight increase in uptake that was comparable between males and females and did not reach statistical significance for any segment. For PSFTOF, the magnitude of change in uptake was greater than for TOF or PSF alone and reached statistical significance in females for heart segments in the anteroseptal and apical anterior walls (see row 5 of the polar maps, segments 2, 8, 13, and 14).

The differences between genders could be due to breasts in the field of view or other factors that correlate with gender. For example, LV myocardial volumes were generally larger for males than for females, as expected (Figure 8). This makes it difficult to decouple the effect of breasts from those of spillover and spatial blurring, which have a greater relative effect for small hearts. Patient characteristics for the two genders are summarized in Table 1. Differences in weight and LV myocardial volume were statistically significant (both $P<.05$), while differences in BMI, cross-sectional area and age were not.

Results by LV myocardial volume. For TOF iterative reconstructions, the change in uptake was greater in patient groups with a smaller LV size (Figure 6, rows 1 and 2). Once again there were increases in the septal wall area that reached statistical significance in AHA segments 8 and 14. With PSF modeling, the slight increase in uptake was comparable among patient groups but was not statistically significant (Figure 6, rows 3 and 4). For PSFTOF, a similar trend as

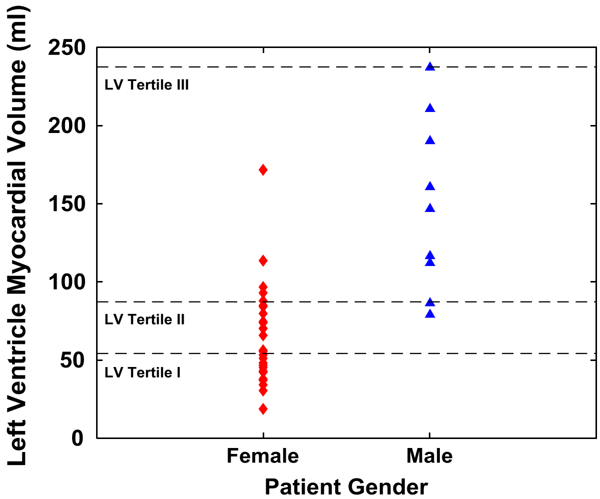

Figure 8. LV myocardial volume distribution for males and females. Dashed lines represent the grouping into tertiles based on LV size.

with TOF was observed, with slightly larger increases in perfusion (Figure 6, row 5). Patient characteristics for the LV size tertiles are summarized in Table 4. Weight was smaller in the LV size-I group (P=.05) and the distribution of male and female patients was different in the LV size-III group, with more males and fewer females (P=.004).

Quantitative Analysis, Summed Scores

The differences in SRS, SSS, and SDS between the reconstruction algorithms were compared on a pairwise basis for all subjects (Table 5) and for BMI, patient cross-sectional area, gender, and LV myocardial volume subgroups (Tables 6, 7, 8, and 9) using LMMs.

Over all subjects (Table 5), the mean SRS and SSS were significantly smaller for reconstructions with TOF compared with reconstructions without TOF (OSEM-TOF vs. OSEM, PSFTOF vs. PSF, PSFTOF vs. OSEM). The magnitude of these decreases ranged between 2.4 and 3.0 and was about the same for SRS and SSS; as a result, the mean SDS differences were near zero and not significantly different. The mean SRS, SSS, and SDS were not significantly different between PSF and non-PSF reconstructions (PSF vs. OSEM, PSFTOF vs. OSEMTOF). These findings are consistent with qualitative polar map and quantitative segmental analyses.

For BMI groups (Table 6), all significant changes in SRS and SSS were the result of including TOF in image reconstruction. Significant changes were observed only for the BMI-I and BMI-II tertiles. The magnitude of significant decreases ranged between 2.9 and 4.3. There were no significant changes in SDS in any BMI tertile for any reconstruction method.

For cross-sectional area groups (Table 7), again all significant differences in SRS and SSS were the result of including TOF in image reconstruction, though TOF did not always result in a significant difference. The number of comparisons for which the differences achieved statistical significance was one for tertile I, 3 for tertile II, and 5 for tertile III. The significant decreases with TOF ranged between 2.8 and 3.4. There were no significant changes in SDS for any cross-sectional area tertile or any reconstruction method.

For gender groups (Table 8), there were only significant changes for females. These occurred only for SRS and SSS when TOF was additionally included in image reconstruction. The magnitude of the significant decreases ranged between 3.1 and 4.0. There were no significant changes in SDS.

For LV myocardial volume groups (Table 9), there were changes in SRS for tertiles I and II and in SSS for tertiles II and III. All were associated with the application of TOF reconstruction, in some cases with PSF as well. The magnitude of the significant decreases in SRS and SSS ranged between 2.7 and 4.9. There were no significant changes in SDS.

DISCUSSION

This study evaluated the effects of TOF and PSF modeling on ^{82}Rb myocardial perfusion PET in obese patients. The most striking qualitative effects with TOF (Figures 1, 2) are (1) improved visual uniformity of the polar maps, (2) increased amplitudes in the septal wall, and (3) reduction in visual appearance of perfusion defects. For observation (1), improved uniformity is likely due to a reduction in artifact strength when there is mismatch between the emission and attenuation maps. The septal wall may be more sensitive to mismatch effects, which could account for observation (2), and many of the perfusion defects in the study population are in the septal wall. A relative increase in septal wall perfusion with TOF is consistent with previous observations.[22,23] The effect of TOF is particularly evident in the quantitative 17-segment analyses when patients are grouped by size (Figures 3, 4). Septal wall perfusion increases by up to about 10% with TOF and is greater for larger patients. The increase with body size is more evident when patients are grouped by cross-sectional area of transaxial slices containing the heart. This is physically reasonable because PET-CT mismatch affecting attenuation and scatter correction is expected to be larger with more body mass in the scanner FOV.

Table 4. Patient groups by LV myocardial volume

Variable	LV Size-I (N=12)	LV Size-II (N=12)	LV Size-III (N=12)	P value
Gender				0.004[2]*
Male	0	2	7	
Female	12	10	5	
Weight (kg)				0.05[1]
Mean± SD	116.98±24.09	144.02±28.17	147.9±35.66	
Median [Q1, Q3]	107.27 [98.77, 142.01]	139.72 [128.22, 147.13]	139.02 [122.3, 171.9]	
Min, max	85.6, 156.64	115.45, 218	105, 225.45	
BMI (kg/m^2)				
Mean± SD	43.09±7.9	49.97±8.1	49.26±11.43	0.15[1]
Median [Q1, Q3]	43.41 [37.9, 46.94]	52.09 [45.19, 55.22]	46.92 [40.35, 55.68]	
Min, max	32.46, 57.19	36.01, 63.87	37.36, 75.57	
LV myocardial volume (mL)				< 0.001[1]*
Mean± SD	40.71±9.74	73.42±10.39	144.71±49.51	
Median [Q1, Q3]	42.5 [36.38, 47.38]	74.25 [68.88, 80.75]	131.5 [108.25, 176.12]	
Min, max	18.5, 53	55.5, 86.5	88, 237.5	
Area, transaxial slice containing the heart (cm^2)				0.6[1]
Mean± SD	1108.04±236.87	1187.75±172.24	1125.28±257.19	
Median [Q1, Q3]	1108.52 [1051.79, 1185.57]	1148.54 [1112.31, 1225.71]	1116.77 [959.27, 1280.77]	
Min, max	531.86, 1548.27	905.49, 1557.89	732.99, 1662.26	
Age (year)				0.87[1]
Mean± SD	56.58±6.75	56.92±11.7	54.25±8.9	
Median [Q1, Q3]	55 [51.75, 63]	56 [49, 62.75]	56.5 [47.25, 60]	
Min, max	46, 69	41, 82	37, 66	

*P value<.05
[1]Kruskal-Wallis H test
[2]Fisher's exact test

There are differences in the effect of TOF between males and females. The increase in septal wall perfusion with TOF is larger and only statistically significant for females (Figure 5). With females, the breasts contribute to soft tissue mass in the cardiac FOV and move with respiration. Thus, the mismatch between PET and CT images may be greater on average for females, possibly accounting for the larger effect of TOF in minimizing the inconsistencies. Since scatter is greater as body mass increases and scatter correction uses the attenuation map, TOF may also partially compensate for errors in scatter correction due to emission-attenuation map mismatch. With our limited dataset it is not possible to decouple the influence of gender-related effects from heart size (Figure 8).

There are technical factors that make scatter correction more challenging for large patients, in particular the fitting and scaling of a simulated scatter tails to the observed scatter tails. For the Biograph mCT the x-ray CT scan for attenuation correction is reconstructed out

Table 5. Comparison of summed score statistics over all patients

All subjects (n=36) Variable	Reconstruction Method OSEM	OSEMTOF	PSF	PSFTOF	Difference	P value[1]
SRS	9.97±6.14	7.43±5.61	10.29±6.45	7.56±5.59		
Comparison	x	x			−2.53±4.26	0.001*
Comparison	x		x		0.33±1.37	0.964
Comparison	x			x	−2.41±3.96	0.002*
Comparison		x	x		2.86±4.91	< 0.001*
Comparison		x		x	0.12±1.51	0.998
Comparison			x	x	−2.74±4.63	< 0.001*
SSS	11.36±8.40	8.42±6.95	11.19±8.35	8.33±6.94		
Comparison	x	x			−2.94±3.93	< 0.001*
Comparison	x		x		−0.16±1.40	0.993
Comparison	x			x	−3.02±3.80	< 0.001*
Comparison		x	x		2.78±4.13	< 0.001*
Comparison		x		x	−0.08±1.40	0.999
Comparison			x	x	−2.86±4.02	< 0.001*
SDS	1.39±5.38	0.98±4.16	0.90±5.25	0.78±4.23		
Comparison	x	x			−0.41±4.14	0.913
Comparison	x		x		−0.49±1.32	0.860
Comparison	x			x	−0.61±3.64	0.757
Comparison		x	x		−0.08±4.33	0.999
Comparison		x		x	−0.20±1.90	0.988
Comparison			x	x	−0.12±3.74	0.997

The two "x" marks in a given row indicate which two of the four image reconstruction methods are compared
Entries are mean±SD
*P value<.05
[1]P value from Scheffé method

to a diameter of 78 cm (the FOV for clinical diagnosis is 50 cm), which is the patient bore diameter of the scanner. The PET activity is reconstructed out to a 70 cm diameter field of view. The extension of single scatter simulation to TOF scatter correction implemented by Siemens is described in Ref.[32] For our study, the largest lateral dimension of a patient in a transaxial slice containing the heart had a mean of 55.2 cm, a median of 53.5 cm, and a range of 38.4-69.0 cm. The corresponding largest anterior-posterior dimension had a mean of 32.0 cm, a median of 32.0 cm, and a range of 22.4-39.6 cm. On average, the patients filled 30% (range 14-43%) of the PET FOV (using data from Table 1 and the area inside the 70 cm diameter PET FOV). There were five patients with a small part of the body outside of the 70 cm PET FOV, and this was always part of an arm. The mean distance outside the 70 cm diameter circle was 2.2 cm with a range of 2.0-2.7 cm. For some patients, this would likely have a small effect on scatter correction. Previous work has shown that TOF reconstructions are less sensitive to data inconsistencies than non-TOF reconstructions.[13,14] Perhaps due to its more central location in the body, the septal wall is more sensitive to inconsistencies in scatter, prompt gamma, and attenuation corrections than other parts of the heart, and any resulting bias is partially compensated with TOF image reconstruction. Although the heart was always near the center of the field of view, the large body habitus with part of the body sometimes near the edge and outside of the reconstructed PET FOV makes scatter and prompt gamma correction more difficult and would be a suitable topic for future investigation.

The effect of PSF modeling was a small increase in perfusion averaging 1.5% in almost all heart segments, though this did not reach statistical significance for any segment (Figures 3, 4, 5, and 6). Images were filtered with the clinically used 8-mm FWHM Gaussian filter, which may have diminished the effect of PSF modeling. PSF modeling was approximate because it was based on the system response for ^{18}F,[16] which has a smaller positron range than ^{82}Rb.

Table 6. Summed score statistics by BMI

	BMI Tertile I ($n=12$)					
	Reconstruction method					
Variable	OSEM	OSEMTOF	PSF	PSFTOF	Difference	P value[1]
SRS	12.87±7.50	10.66±7.98	13.24±7.71	10.91±7.56		
Comparison	x	x			−2.21±3.84	0.244
Comparison	x		x		0.37±0.91	0.990
Comparison	x			x	−1.96±2.96	0.349
Comparison		x	x		2.57±4.53	0.129
Comparison		x		x	0.25±1.38	0.997
Comparison			x	x	−2.33±3.68	0.200
SSS	14.95±11.93	11.89±10.14	14.58±12.00	11.64±10.18		
Comparison	x	x			−3.06±4.41	0.019*
Comparison	x		x		−0.37±1.42	0.986
Comparison	x			x	−3.31±4.48	0.009*
Comparison		x	x		2.70±4.34	0.053
Comparison		x		x	−0.25±1.06	0.996
Comparison			x	x	−2.94±4.16	0.027*
SDS	2.08±5.69	1.23±4.06	1.35±5.62	0.74±4.32		
Comparison	x	x			−0.86±3.57	0.864
Comparison	x		x		−0.74±1.60	0.909
Comparison	x			x	−1.35±3.57	0.609
Comparison		x	x		0.12±4.04	1.000
Comparison		x		x	−0.49±2.02	0.971
Comparison			x	x	−0.61±3.57	0.945

	BMI Tertile II ($n=12$)					
	Reconstruction method					
Variable	OSEM	OSEMTOF	PSF	PSFTOF	Difference	P value[1]
SRS	10.05±4.81	6.37±3.28	10.54±5.81	6.25±3.33		
Comparison	x	x			−3.68±4.28	0.009*
Comparison	x		x		0.49±1.92	0.977
Comparison	x			x	−3.80±4.84	0.006*
Comparison		x	x		4.17±5.39	0.002*
Comparison		x		x	−0.12±1.17	1.000
Comparison			x	x	−4.29±5.66	0.001*
SSS	11.52±6.27	8.21±3.10	11.89±5.96	7.72±3.66		
Comparison	x	x			−3.31±4.21	0.009*
Comparison	x		x		0.37±1.67	0.986
Comparison	x			x	−3.80±3.84	0.002*
Comparison		x	x		3.68±4.37	0.003*
Comparison		x		x	−0.49±0.96	0.968
Comparison			x	x	−4.17±4.06	< 0.001*
SDS	1.47±6.75	1.84±4.02	1.35±6.62	1.47±4.52		
Comparison	x	x			0.37±4.44	0.987
Comparison	x		x		−0.12±1.17	1.000
Comparison	x			x	0.00±4.11	1.000
Comparison		x	x		−0.49±4.13	0.971
Comparison		x		x	−0.37±1.11	0.987
Comparison			x	x	0.12±3.79	1.000

Table 6. continued

	BMI Tertile III (*n*=12)					
	Reconstruction method					
Variable	**OSEM**	**OSEMTOF**	**PSF**	**PSFTOF**	**Difference**	***P* value[1]**
SRS	6.99±4.66	5.27±2.84	7.11±4.34	5.51±3.55		
Comparison	x	x			−1.72±4.73	0.472
Comparison	x		x		0.12±1.17	1.000
Comparison	x			x	−1.47±3.81	0.604
Comparison		x	x		1.84±4.90	0.409
Comparison		x		x	0.25±1.97	0.997
Comparison			x	x	−1.59±4.27	0.538
SSS	7.60±3.65	5.15±4.04	7.11±3.31	5.64±4.01		
Comparison	x	x			−2.45±3.40	0.096
Comparison	x		x		−0.49±0.96	0.968
Comparison	x			x	−1.96±3.03	0.254
Comparison		x	x		1.96±3.83	0.254
Comparison		x		x	0.49±1.92	0.968
Comparison			x	x	−1.47±3.71	0.515
SDS	0.61±3.57	−0.12±4.50	0.00±3.32	0.12±4.09		
Comparison	x	x			−0.74±4.59	0.909
Comparison	x		x		−0.61±1.17	0.945
Comparison	x			x	−0.49±3.40	0.971
Comparison		x	x		0.12±5.11	1.000
Comparison		x		x	0.25±2.42	0.996
Comparison			x	x	0.12±4.13	1.000

The two "x" marks in a given row indicate which two of the four image reconstruction methods are compared
Entries are mean±SD
**P* value<.05
[1]*P* value from Scheffé method

TOF plus PSF modeling combined the individual effects of TOF and PSF, with the largest amplitude increases in the septal wall. The magnitude of the effects appears roughly additive and the response is dominated by the TOF effects.

TOF generally decreased SRS and SSS, with significant mean decreases between 2.4 and 3.0 (Table 5; OSEMTOF vs. OSEM, PSFTOF vs. PSF). This could affect patient risk stratification and move some patients into a less severe category. Changes in SRS and SSS tended to be in the same direction, with the result that SDS values tended to remain unchanged. The addition of PSF in image reconstruction (PSF vs OSEM, PSFTOF vs OSEMTOF) did not significantly change SRS, SSS, or SDS. The effect of TOF on SRS and SSS was greater for females (Table 8).

Reconstructed images used coincidence data from 1.5 to 8 minutes after Rb-82 injection as is standard of care at our institution. Use of an earlier starting time would result in an increased number of counts at the expense of decreased blood pool clearance, while a later starting time would result in fewer counts with increased blood pool clearance. Adjustment of the starting time would thus affect the image noise. It is likely that the study results would be similar if the starting time were adjusted, both because of the spatial smoothing employed as part of image reconstruction and because the quantitative analysis used a 17-segment model rather than a finer cardiac subdivision.

This was a clinical study and the true perfusion is not known. In general, however, better modeling of the physics of photon transport and detection within the body and PET instrumentation in image reconstruction will result in more accurate estimation of in vivo radiopharmaceutical uptake. In a recent study of anthropomorphic cardiac-torso phantoms of large patients, we showed that incorporating TOF and PSF modeling in image reconstruction improves quantitation accuracy.[29] TOF reduced artifacts associated with deliberate spatial mismatch between the emission scan and the x-ray CT

Table 7. Summed score statistics by patient cross-sectional area in the FOV

Variable	Area tertile I (*n*=12)					
	Reconstruction method					
Variable	OSEM	OSEMTOF	PSF	PSFTOF	Difference	*P* value[1]
SRS	10.78±7.43	8.70±8.65	11.03±8.02	8.70±8.38		
Comparison	x	x			−2.08±3.52	0.314
Comparison	x		x		0.25±1.97	0.997
Comparison	x			x	−2.08±3.04	0.314
Comparison		x	x		2.33±5.00	0.218
Comparison		x		x	0.00±1.25	1.000
Comparison			x	x	−2.33±4.41	0.218
SSS	12.87±11.31	10.42±9.62	12.62±11.55	9.93±9.76		
Comparison	x	x			−2.45±2.90	0.105
Comparison	x		x		−0.25±1.76	0.996
Comparison	x			x	−2.94±2.66	0.032*
Comparison		x	x		2.21±3.68	0.174
Comparison		x		x	−0.49±0.72	0.970
Comparison			x	x	−2.70±3.31	0.060
SDS	2.08±6.88	1.72±4.15	1.59±7.33	1.23±4.47		
Comparison	x	x			−0.37±4.48	0.987
Comparison	x		x		−0.49±1.14	0.971
Comparison	x			x	−0.86±4.32	0.866
Comparison		x	x		−0.12±4.79	1.000
Comparison		x		x	−0.49±1.45	0.971
Comparison			x	x	−0.37±4.48	0.987

Variable	Area tertile II (*n*=12)					
	Reconstruction method					
Variable	OSEM	OSEMTOF	PSF	PSFTOF	Difference	*P* value[1]
SRS	10.66±5.47	7.97±3.63	10.91±5.96	7.97±3.63		
Comparison	x	x			−2.70±4.25	0.114
Comparison	x		x		0.25±0.85	0.997
Comparison	x			x	−2.70±5.13	0.114
Comparison		x	x		2.94±4.61	0.070
Comparison		x		x	0.00±1.09	1.000
Comparison			x	x	−2.94±5.47	0.070
SSS	12.50±7.46	9.56±5.70	12.38±7.46	9.68±6.13		
Comparison	x	x			−2.94±4.90	0.032*
Comparison	x		x		−0.12±1.17	0.999
Comparison	x			x	−2.82±4.79	0.044*
Comparison		x	x		2.82±5.19	0.044*
Comparison		x		x	0.12±1.47	0.999
Comparison			x	x	−2.70±5.31	0.060
SDS	1.84±5.33	1.59±4.04	1.47±4.52	1.72±4.56		
Comparison	x	x			−0.25±3.48	0.996
Comparison	x		x		−0.37±1.11	0.987
Comparison	x			x	−0.12±3.46	1.000
Comparison		x	x		−0.12±2.97	1.000
Comparison		x		x	0.12±1.32	1.000
Comparison			x	x	0.25±3.12	0.996

Table 7. continued

Variable	Area tertile III (*n*=12)					
	Reconstruction method					
	OSEM	OSEMTOF	PSF	PSFTOF	Difference	*P* value[1]
SRS	8.46±5.58	5.64±2.57	8.95±5.45	6.00±3.46		
Comparison	x	x			−2.82±5.19	0.090
Comparison	x		x		0.49±1.14	0.978
Comparison	x			x	−2.45±3.78	0.178
Comparison		x	x		3.31±5.47	0.030*
Comparison		x		x	0.37±2.09	0.991
Comparison			x	x	−2.94±4.30	0.070
SSS	8.70±5.41	5.27±3.46	8.58±4.64	5.39±2.53		
Comparison	x	x			−3.43±4.03	0.007*
Comparison	x		x		−0.12±1.32	0.999
Comparison	x			x	−3.31±3.97	0.011*
Comparison		x	x		3.31±3.61	0.011*
Comparison		x		x	0.12±1.82	0.999
Comparison			x	x	−3.19±3.48	0.016*
SDS	0.25±3.75	−0.37±4.30	−0.37±3.33	−0.61±3.57		
Comparison	x	x			−0.61±4.71	0.946
Comparison	x		x		−0.61±1.71	0.946
Comparison	x			x	−0.86±3.35	0.866
Comparison		x	x		0.00±5.28	1.000
Comparison		x		x	−0.25±2.72	0.996
Comparison			x	x	−0.25±3.81	0.996

The two "x" marks in a given row indicate which two of the four image reconstruction methods are compared
Entries are mean±SD
[1]*P* value from Scheffé method
**P* value<.05

scan used for attenuation correction. It is therefore likely that clinical image reconstructions using TOF and PSF modeling provide the best estimates of myocardial perfusion. Nonetheless, additional phantom studies with perfusion defect inserts may shed additional light on the change in defect sizes observed in the polar map displays of these clinical studies for different image reconstruction methods, particularly for TOF vs. non-TOF reconstructions.

The results of this study show that both TOF and PSF modeling in image reconstruction have measurable effects on qualitative and quantitative observations of perfusion. Clinicians should consider these effects and gender differences when interpreting ^{82}Rb perfusion studies. Further work is needed to investigate the observed dependence on gender. Work is ongoing to study the separate effects of TOF and PSF on absolute myocardial blood flow and flow reserve.

STUDY LIMITATIONS

This is a single-center study with a limited number of patients and the demographics are representative of obese patients presenting for PET MPI at the University of Maryland Medical Center. The patients were enrolled over a period of 12 months and in this study 9 of the patients were male and 27 were female. The gender distribution of obese patients presenting for MPI will differ at other institutions and further work is necessary to assess whether the conclusions of this paper apply to other patient populations.

This study employed clinical settings of iteration number, number of subsets, and post-reconstruction filter and did not systematically evaluate different settings. Convergence to a given noise level, image resolution, or other metric would depend on factors such as administered activity, patient weight, BMI, and other aspects of body habitus or physiology and is likely

Table 8. Summed score statistics by gender

	Male (*n*=9)					
	Reconstruction method					
Variable	OSEM	OSEMTOF	PSF	PSFTOF	Difference	*P* value[1]
SRS	10.29±8.76	10.78±9.30	10.29±8.64	10.13±9.05		
Comparison	x	x			0.49±3.12	0.982
Comparison	x		x		0.00±1.04	1.000
Comparison	x			x	−0.16±3.16	0.999
Comparison		x	x		−0.49±3.75	0.982
Comparison		x		x	−0.65±1.07	0.958
Comparison			x	x	−0.16±3.78	0.999
SSS	14.22±12.50	11.76±10.86	13.24±12.95	11.44±10.70		
Comparison	x	x			−2.45±3.53	0.187
Comparison	x		x		−0.98±1.04	0.857
Comparison	x			x	−2.78±2.79	0.104
Comparison		x	x		1.47±3.75	0.631
Comparison		x		x	−0.33±2.05	0.994
Comparison			x	x	−1.80±3.01	0.461
SDS	3.92±5.04	0.98±4.99	2.94±5.50	1.31±3.48		
Comparison	x	x			−2.94±5.40	0.064
Comparison	x		x		−0.98±1.27	0.848
Comparison	x			x	−2.61±4.21	0.125
Comparison		x	x		1.96±6.24	0.358
Comparison		x		x	0.33±2.52	0.993
Comparison			x	x	−1.63±4.96	0.524

	Female (*n*=27)					
	Reconstruction method					
Variable	OSEM	OSEMTOF	PSF	PSFTOF	Difference	*P* value[1]
SRS	9.86±5.20	6.32±3.26	10.29±5.75	6.70±3.72		
Comparison	x	x			−3.54±4.14	< 0.001*
Comparison	x		x		0.44±1.46	0.937
Comparison	x			x	−3.16±3.97	< 0.001*
Comparison		x	x		3.98±4.79	< 0.001*
Comparison		x		x	0.38±1.56	0.957
Comparison			x	x	−3.59±4.62	< 0.001*
SSS	10.40±6.56	7.30±4.85	10.51±6.35	7.30±5.02		
Comparison	x	x			−3.10±4.11	< 0.001*
Comparison	x		x		0.11±1.41	0.999
Comparison	x			x	−3.10±4.13	< 0.001*
Comparison		x	x		3.21±4.22	< 0.001*
Comparison		x		x	0.00±1.15	1.000
Comparison			x	x	−3.21±4.30	< 0.001*
SDS	0.54±5.30	0.98±3.95	0.22±5.09	0.60±4.49		
Comparison	x	x			0.44±3.33	0.924
Comparison	x		x		−0.33±1.31	0.966
Comparison	x			x	0.05±3.25	1.000
Comparison		x	x		−0.76±3.37	0.691

Table 8. contimud

Variable	Female (*n*=27)					
	Reconstruction method					
	OSEM	OSEMTOF	PSF	PSFTOF	Difference	*P* value[1]
Comparison		x		x	−0.38±1.66	0.947
Comparison			x	x	0.38±3.20	0.947

The two "x" marks in a given row indicate which two of the four image reconstruction methods are compared
Entries are mean±SD
* *P* value<.05
[1]*P* value from Scheffé method

Table 9. Summed score statistics by left ventricular myocardial volume

Variable	LV tertile I (*n*=12)					
	Reconstruction method					
	OSEM	OSEMTOF	PSF	PSFTOF	Difference	*P* value[1]
SRS	9.31±5.22	6.37±3.93	9.93±6.37	6.50±4.23		
Comparison	x	x			−2.94±3.32	0.059
Comparison	x		x		0.61±1.93	0.956
Comparison	x			x	−2.82±3.16	0.077
Comparison		x	x		3.55±4.71	0.012*
Comparison		x		x	0.12±0.98	1.000
Comparison			x	x	−3.43±4.40	0.017*
SSS	9.19±7.10	7.72±5.82	9.80±6.76	7.72±5.92		
Comparison	x	x			−1.47±3.81	0.468
Comparison	x		x		0.61±1.59	0.932
Comparison	x			x	−1.47±3.43	0.468
Comparison		x	x		2.08±3.94	0.165
Comparison		x		x	0.00±0.89	1.000
Comparison			x	x	−2.08±3.46	0.165
SDS	−0.12±6.16	1.35±4.58	−0.12±5.96	1.23±4.85		
Comparison	x	x			1.47±3.76	0.501
Comparison	x		x		0.00±1.40	1.000
Comparison	x			x	1.35±3.23	0.575
Comparison		x	x		−1.47±3.81	0.501
Comparison		x		x	−0.12±1.17	0.999
Comparison			x	x	1.35±3.23	0.575

Variable	LV tertile II (*n*=12)					
	Reconstruction method					
	OSEM	OSEMTOF	PSF	PSFTOF	Difference	*P* value[1]
SRS	10.54±6.11	6.74±2.84	10.42±6.44	7.23±3.40		
Comparison	x	x			−3.80±5.76	0.006*
Comparison	x		x		−0.12±0.98	1.000
Comparison	x			x	−3.31±5.33	0.024*
Comparison		x	x		3.68±6.19	0.009*
Comparison		x		x	0.49±2.20	0.976
Comparison			x	x	−3.19±5.84	0.033*

Table 9. continued

	LV tertile II ($n=12$)					
	Reconstruction method					
Variable	OSEM	OSEMTOF	PSF	PSFTOF	Difference	P value[1]
SSS	12.38±6.19	6.86±4.31	11.64±6.71	7.48±4.41		
Comparison	x	x			−5.51±3.92	< 0.001*
Comparison	x		x		−0.74±1.33	0.888
Comparison	x			x	−4.90±4.66	< 0.001*
Comparison		x	x		4.78±4.78	< 0.001*
Comparison		x		x	0.61±1.82	0.932
Comparison			x	x	−4.17±5.50	< 0.001*
SDS	1.84±4.61	0.12±4.37	1.23±4.47	0.25±4.38		
Comparison	x	x			−1.72±4.10	0.359
Comparison	x		x		−0.61±1.47	0.938
Comparison	x			x	−1.59±3.16	0.428
Comparison		x	x		1.10±4.40	0.722
Comparison		x		x	0.12±2.77	0.999
Comparison			x	x	−0.98±3.28	0.789

	LV tertile III ($n=12$)					
	Reconstruction method					
Variable	OSEM	OSEMTOF	PSF	PSFTOF	Difference	P value[1]
SRS	10.05±7.39	9.19±8.46	10.54±7.09	8.95±8.16		
Comparison	x	x			−0.86±2.90	0.889
Comparison	x		x		0.49±0.96	0.976
Comparison	x			x	−1.10±2.95	0.790
Comparison		x	x		1.35±3.52	0.668
Comparison		x		x	−0.25±1.06	0.997
Comparison			x	x	−1.59±3.52	0.535
SSS	12.50±11.31	10.66±9.62	12.13±11.31	9.80±9.76		
Comparison	x	x			−1.84±2.88	0.265
Comparison	x		x		−0.37±0.91	0.984
Comparison	x			x	−2.70±2.42	0.036*
Comparison		x	x		1.47±3.01	0.468
Comparison		x		x	−0.86±0.98	0.834
Comparison			x	x	−2.33±2.54	0.095
SDS	2.45±5.37	1.47±3.71	1.59±5.52	0.86±3.68		
Comparison	x	x			−0.98±4.18	0.789
Comparison	x		x		−0.86±0.98	0.848
Comparison	x			x	−1.59±3.94	0.428
Comparison		x	x		0.12±4.71	0.999
Comparison		x		x	−0.61±1.47	0.938
Comparison			x	x	−0.74±4.46	0.899

The two "x" marks in a given row indicate which two of the four image reconstruction methods are compared
Entries are mean±SD
* P value<.05
[1] P value from Scheffé method

patient-dependent, though certain fixed values of iterations, subsets, and post-reconstruction filter are commonly employed in clinical practice, with some sites using fewer iterations with TOF reconstruction. Certain image reconstruction settings that were used in this study, such as 21 subsets for non-TOF image reconstructions, were possible with the Siemens e7 software toolkit and may not be available as part of the clinical software release on the Biograph mCT. A thorough investigation of image reconstruction parameters is non-trivial and would merit a separate investigation. The PET scans and implementation of TOF and PSF modeling used hardware and software of a single vendor (Siemens Medical Solutions) and applicability of the findings for PET systems of other manufacturers would need to be validated.

NEW KNOWLEDGE GAINED

The individual and combined effects of TOF and PSF modeling in image reconstruction were investigated for ^{82}Rb MPI in obese patients. The major effect of TOF was improved visual uniformity of polar maps and greater perfusion in the septal wall as the body cross-sectional area in the PET scanner FOV increased. This latter effect was more prominent for females than males. PSF modeling generally resulted in a small increase in perfusion in all cardiac segments. The general effect of TOF modeling was to decrease SRS and SSS, which could affect patient risk stratification. These changes were about the same magnitude and so SDS remained about the same. With PSF modeling SRS, SSS, and SDS were largely unchanged. This paper adds to the knowledge of how advanced image reconstruction algorithms affect ^{82}Rb myocardial perfusion imaging of obese patients.

CONCLUSION

TOF and PSF modeling in image reconstruction both had significant effects on ^{82}Rb PET MPI of obese patients. TOF improved visual uniformity of polar maps, increased amplitudes in the septal wall, and reduced the visual appearance of perfusion defects. Septal wall perfusion increased by up to about 10% with TOF and this increase was greater for larger patients. The increase was more evident for patients grouped by body cross-sectional area in transaxial slices containing the heart than by BMI. The increase in septal wall perfusion with TOF was greater for females than males. The effect of PSF modeling was a small increase in perfusion in almost all heart segments, averaging about 1.5%. TOF modeling generally decreased SRS and SSS, which could affect risk stratification. These changes were about the same magnitude and so SDS remained about the same. With PSF modeling, SRS, SSS, and SDS were largely unchanged. Clinicians should consider effects of TOF and PSF modeling and gender differences when interpreting ^{82}Rb-82 perfusion studies.

Disclosure

This work was supported in part by Siemens Medical Solutions. P.K.R. Dasari, V. Dilsizian, M.F. Smith, and Y. Liang were employees of the University of Maryland, Baltimore when this research was conducted. J.P. Jones and M.E. Casey were employees of Siemens Healthineers.

References

1. Bateman TM, Heller GV, McGhie AI, Friedman JD, Case JA, Bryngelson JR, et al. Diagnostic accuracy of rest/stress ECG-gated Rb-82 myocardial perfusion PET: Comparison with ECG-gated Tc-99m sestamibi SPECT. J Nucl Cardiol. 2006;13:24–33.
2. Flotats A, Bravo PE, Fukushima K, Chaudhry MA, Merrill J, Bengel FM. 82Rb PET myocardial perfusion imaging is superior to 99mTc-labelled agent SPECT in patients with known or suspected coronary artery disease. Eur J Nucl Med Mol I. 2012;39:1233–9.
3. Sampson UK, Dorbala S, Limaye A, Kwong R, Di Carli MF. Diagnostic accuracy of rubidium-82 myocardial perfusion imaging with hybrid positron emission tomography/computed tomography in the detection of coronary artery disease. J Am Coll Cardiol. 2007;49:1052–8.
4. Freedman N, Schechter D, Klein M, Marciano R, Rozenman Y, Chisin R. SPECT attenuation artifacts in normal and overweight persons: Insights from a retrospective comparison of Rb-82 positron emission tomography and Tl-201 SPECT myocardial perfusion imaging. Clin Nucl Med. 2000;25:1019–23.
5. Mc Ardle BA, Dowsley TF, deKemp RA, Wells GA, Beanlands RS. Does rubidium-82 PET have superior accuracy to SPECT perfusion imaging for the diagnosis of obstructive coronary disease? A systematic review and meta-analysis. J Am Coll Cardiol. 2012;60:1828–37.
6. Chow BJW, Dorbala S, Di Carli MF, Merhige ME, Williams BA, Veledar E, et al. Prognostic value of PET myocardial perfusion imaging in obese patients. J Am Coll Cardiol Img. 2014;7:278–87.
7. Karp JS, Surti S, Daube-Witherspoon ME, Muehllehner G. Benefit of time-of-flight in PET: Experimental and clinical results. J Nucl Med. 2008;49:462–70.
8. Conti M. Focus on time-of-flight PET: The benefits of improved time resolution. Eur J Nucl Med Mol I. 2011;38:1147–57.
9. Lois C, Jakoby BW, Long MJ, Hubner KF, Barker DW, Casey ME, et al. An assessment of the impact of incorporating time-of-flight Information into clinical PET/CT imaging. J Nucl Med. 2010;51:237–45.
10. Taniguchi T, Akamatsu G, Kasahara Y, Mitsumoto K, Baba S, Tsutsui Y, et al. Improvement in PET/CT image quality in overweight patients with PSF and TOF. Ann Nucl Med. 2015;29:71–7.
11. Kadrmas DJ, Casey ME, Conti M, Jakoby BW, Lois C, Townsend DW. Impact of time-of-flight on PET tumor detection. J Nucl Med. 2009;50:1315–23.
12. Daube-Witherspoon ME, Surti S, Perkins AE, Karp JS. Determination of accuracy and precision of lesion uptake measurements in

human subjects with time-of-flight PET. J Nucl Med. 2014;55:602–7.
13. Conti M. Why is TOF PET reconstruction a more robust method in the presence of inconsistent data? Phys Med Biol. 2011;56:155–68.
14. Turkington TG, Wilson JM. Attenuation artifacts and time-of-flight PET. 2009 IEEE Nuclear Science Symposium Conference Record, Vols 1-5. 2009:2997-9.
15. Bai C, Andreyev A, Hu Z, Maniawski P, Zhang J, Knopp M. TOF reconstruction for improved quantitative accuracy in PET/CT studies with misalignment. J Nucl Med. 2016;57:478.
16. Panin VY, Kehren F, Michel C, Casey M. Fully 3-D PET reconstruction with system matrix derived from point source measurements. IEEE Trans Med Imaging. 2006;25:907–21.
17. Walker MD, Asselin MC, Julyan PJ, Feldmann M, Talbot PS, Jones T, et al. Bias in iterative reconstruction of low-statistics PET data: Benefits of a resolution model. Phys Med Biol. 2011;56:931.
18. Tong S, Alessio AM, Kinahan PE. Noise and signal properties in PSF-based fully 3D PET image reconstruction: An experimental evaluation. Phys Med Biol. 2010;55:1453.
19. Rahmim A, Qi J, Sossi V. Resolution modeling in PET imaging: Theory, practice, benefits, and pitfalls. Med Phys. 2013;40:064301.
20. Tong S, Alessio AM, Thielemans K, Stearns C, Ross S, Kinahan PE. Properties and mitigation of edge artifacts in PSF-based PET reconstruction. IEEE Trans Nucl Sci. 2011;58:2264–75.
21. Le Meunier L, Slomka PJ, Dey D, Ramesh A, Thomson LEJ, Hayes SW, et al. Enhanced definition PET for cardiac imaging. J Nucl Cardiol. 2010;17:414–26.
22. Armstrong IS, Tonge CM, Arumugam P. Impact of point spread function modeling and time-of-flight on myocardial blood flow and myocardial flow reserve measurements for rubidium-82 cardiac PET. J Nucl Cardiol. 2014;21:467–74.
23. DiFilippo FP, Brunken RC. Impact of time-of-flight reconstruction on cardiac PET images of obese patients. Clin Nucl Med. 2017;42:e103–8.
24. Tipnis S, Hu Z, Gagnon D, O' Donnell J. Time-of-flight PET for Rb-82 cardiac perfusion imaging. J Nucl Med. 2008;49:74P.
25. Oldan JD, Shah SN, Brunken RC, DiFilippo FP, Obuchowski NA, Bolen MA. Do myocardial PET-MR and PET-CT FDG images provide comparable information? J Nucl Cardiol. 2016;23:1102–9.
26. Armstrong IS, Tonge CM, Arumugam P. Assessing time-of-flight signal-to-noise ratio gains within the myocardium and subsequent reductions in administered activity in cardiac PET studies. J Nucl Cardiol 2017.
27. Wells RG, deKemp RA. Does time-of-flight improve image quality in the heart? J Nucl Cardiol 2017.
28. Budinger TF. Time-of-flight positron emission tomography: Status relative to conventional PET. J Nucl Med. 1983;24:73–8.
29. Dasari PKR, Jones JP, Casey ME, Smith MF. The effect of time-of-flight and point spread function modeling on quantitative cardiac PET of large patients: Phantom studies. IEEE Trans Rad Plasma Med Sci. 2017;1:416–25.
30. Jakoby BW, Bercier Y, Conti M, Casey ME, Bendriem B, Townsend DW. Physical and clinical performance of the mCT time-of-flight PET/CT scanner. Phys Med Biol. 2011;56:2375–89.
31. Tout D, Tonge CM, Muthu S, Arumugam P. Assessment of a protocol for routine simultaneous myocardial blood flow measurement and standard myocardial perfusion imaging with rubidium-82 on a high count rate positron emission tomography system. Nucl Med Commun. 2012;33:1202–11.
32. Watson CC. Extension of single scatter simulation to scatter correction of time-of-flight PET. IEEE Trans Nucl Sci. 2007;54:1679–86.
33. Esteves FP, Nye JA, Khan A, Folks RD, Halkar RK, Garcia EV, et al. Prompt-gamma compensation in Rb-82 myocardial perfusion 3D PET/CT. J Nucl Cardiol. 2010;17:247–53.
34. Cerqueira MD, Weissman NJ, Dilsizian V, Jacobs AK, Kaul S, Laskey WK, et al. Standardized myocardial segmentation and nomenclature for tomographic imaging of the heart: A statement for healthcare professionals from the Cardiac Imaging Committee of the Council on Clinical Cardiology of the American Heart Association. Circulation. 2002;105:539–42.
35. Ficaro EP, Lee BC, Kritzman JN, Corbett JR. Corridor4DM: The Michigan method for quantitative nuclear cardiology. J Nucl Cardiol. 2007;14:455–65.
36. Hachamovitch R, Berman D, Shaw LJ, Germano G, Mieres JH. Risk stratification and patient management. In: Dilsizian V, Narula J, editors. Atlas of nuclear cardiology. 4th ed. New York: Springer; 2013. p. 247–88.
37. Germano G, Kavanagh P, Waechter P, Areeda J, Van Kriekinge S, Sharir T, et al. A new algorithm for the quantitation of myocardial perfusion SPECT. I: Technical principles and reproducibility. J Nucl Med. 2000;41:712–9.
38. Wawrzyniak A, Dilsizian V, Krantz D, Harris K, Smith M, Shankovich A, et al. High concordance between mental stress-induced and adenosine-induced myocardial ischemia assessed using SPECT in heart failure patients: Hemodynamic and biomarker correlates. J Nucl Med. 2015;56:1527–33.